On-surface Hydrogen-induced Covalent Coupling of Polycyclic Aromatic Hydrocarbons via a Super-hydrogenated Intermediate

Carlos Sánchez-Sánchez[1*], José Ignacio Martínez[1], Nerea Ruiz del Arbol[1], Pascal Ruffieux[2], Roman Fasel[2,3], María Francisca López[1], Pedro L. de Andres[1], José Ángel Martín-Gago[1*]

[1]*ESISNA group, Materials Science Factory, Institute of Material Science of Madrid (ICMM-CSIC). Sor Juana Inés de la Cruz 3, 28049 Madrid (Spain).*

[2]*Empa, Swiss Federal Laboratories for Materials Science and Technology,nanotech@surfaces Laboratory, Ueberlandstrasse 129, 8600 Duebendorf (Switzerland).*

[3]*Department of Chemistry and Biochemistry, University of Bern, Freiestrasse 3, 3012 Bern (Switzerland).*

Abstract

The activation, hydrogenation, and covalent coupling of polycyclic aromatic hydrocarbons (PAHs) are processes of great importance in fields like chemistry, energy, biology, or health, among others. So far, they are based on the use of catalysts which drive and increase the efficiency of the thermally- or light-induced reaction. Here, we report on the catalyst-free covalent coupling of non-functionalized PAHs adsorbed on a relatively inert surface in presence of atomic hydrogen. The underlying mechanism has been characterized by high-resolution scanning tunnelling microscopy and rationalized by density functional theory calculations. It is based on the formation of intermediate radical-like species upon hydrogen-induced molecular super-hydrogenation which favors the covalent binding of PAHs in a thermally-activated process resulting in large coupled molecular nanostructures. The mechanism proposed in this work opens a door toward the direct formation of covalent, PAH-based, bottom-up synthetized nano-architectures on technologically relevant inert surfaces.

Keywords: super-hydrogenation, polycyclic aromatic hydrocarbons, covalent coupling, atomic hydrogen, on-surface chemistry.

Introduction

Polycyclic aromatic hydrocarbons (PAHs) –organic compounds constituted by carbon aromatic rings and hydrogen– are ubiquitous in society.[1] They are routinely used in a wide variety of scientific and technological fields such as fundamental chemistry, drugs production, or chemical and petrochemical industry, among many others. The simplest PAH, benzene, is one of the main precursors for the chemical industry, with a world

production in the range of tens of million tons per year.[2] PAHs are commonly found in air and soil as a consequence of natural processes and human activity, where they constitute an important health risk.[3] However, their presence is not limited to Earth. PAHs of different sizes have been detected in the outer space,[4,5] where their formation mechanisms are still under intense debate.[6,7] Interestingly, interstellar PAHs have been invoked as crucial precursor both in the exogenous origin of life, through dehydrogenation and coupling processes,[8] and as one of the key players in the formation of interstellar hydrogen *via* super-hydrogenated intermediate species.[7,9,10]

Most of the above mentioned scientific or technological processes require of a common intermediate step in which PAHs are to be activated. However, despite being of unarguable importance,[11] the atomistic mechanisms of PAH super-hydrogenation (addition of an extra hydrogen atom to the PAH) and activation are still poorly understood. It is known that PAH activation reactions through dehydrogenation are unlikely processes which require overcoming an activation energy barrier given by the strength of the C-H bond, typically in the range of 3.5 – 4.5 eV.[12] Such energy barriers prevent the easy dehydrogenation of PAHs at room temperature (RT) even for reactions with an advantageous energy balance (exothermic). To overcome this issue, it is a common practice to include a catalyst.[13]

One of the strategies followed to activate otherwise stable PAHs is the formation of arenium ion intermediates in electrophilic aromatic substitution reactions by the attachment of an extra proton or functional group to one of the peripheral C atoms of the PAH.[14] This addition induces a local sp^2 to sp^3 transition which breaks the aromaticity of the molecule, delocalizing positive charge in the π system and making the molecule more reactive. Here, we shall argue that the addition of atomic hydrogen plays a similar role in our molecules.

The recent advent of *On-surface Synthesis*, the use of well-controlled ultra-high vacuum (UHV) environments and well-defined single-crystalline metallic surfaces, and the application of Surface Science techniques to the characterization of chemical reactions has afforded a deeper comprehension of the reaction mechanisms operating at the molecular level.[15] Furthermore, it has allowed the emergence of new covalent coupling reactions yielding unprecedented low-dimensional nanostructures, otherwise unattainable *via* traditional solution-based chemistry.[16–19] Dehydrogenation and cyclo-dehydrogenation are among the pioneering and more extensively used on-surface reactions. They have been applied to the fabrication of 0D fullerenes,[20,21] nanodomes,[22–24] nano-graphene,[25–29] and nanostructured molecules;[30] 1D graphene nanoribbons;[31] or even 2D networks and full graphene,[32,33] to only name some of them. However, this rapidly increasing field suffers from a limited number of substrates where the reaction may occur and, often, the interaction of the reaction product with the underlying

metal substrate significantly modifies its properties, which preclude their further use.

Herein, we have made use of the unique access to atomic-scale information provided by On-surface Synthesis to characterize and exploit an unprecedented mechanism for the covalent coupling of PAHs directly on relatively inert surfaces. This is a three-steps process. Firstly, surface deposited PAHs are activated by super-hydrogenation upon exposure to atomic hydrogen. Secondly, two super-hydrogenated PAHs diffuse and collide at radical-like carbon positions (next neighbors to the super-hydrogenated site), leading to the formation of new intermolecular covalent C-C bonds; and third, they release the extra H in the form of two hydrogen molecules (see Figure 1b for a schematic view of the whole process). The relevance of this work is two-fold: (1) It aims at unveiling the atomistic mechanisms for super-hydrogenation and covalent coupling of PAHs on surfaces, and (2) it makes use of these ideas to achieve organic nanostructures by intermolecular covalent coupling of PAHs. Our method paves the way toward the activation and further covalent coupling of aromatic organic molecules on substrates characterized by a low reactivity, thus increasing their potential technological interest.

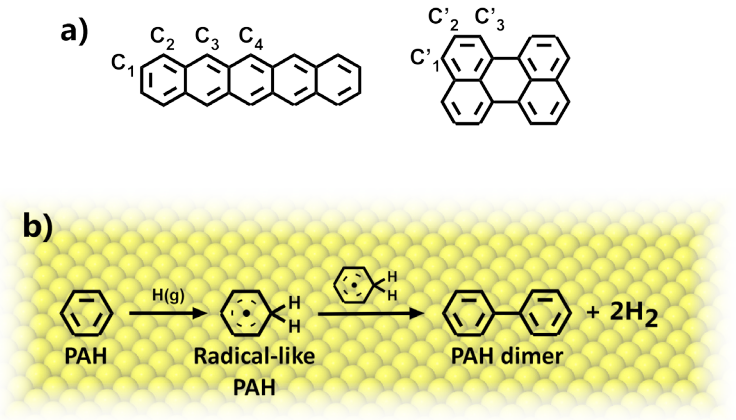

Figure 1.- a) Schematic representation of the pentacene (left) and perylene (right) molecules used in these experiments and the notation for peripheral C atoms. **b)** Schematic representation of the proposed three-step reaction mechanism resulting in the formation of covalent molecular nanostructures and the release of molecular hydrogen. It consists on the super-hydrogenation of the PAH and the subsequent interaction of two activated PAHs to form a covalent dimer.

Results and Discussion

To show the viability of our process, we have chosen as model systems two prototypical PAHs –pentacene and perylene– and a commonly used metallic substrate in On-surface Synthesis –Au(111). Such a choice is rationalized by the weak molecule-surface interaction, which allows intact adsorption at RT and molecular desorption in the temperature range between 375 – 525 K, as we shall see below. For the sake of clarity, we present a detailed analysis for the pentacene case, while further corroboration of our results with perylene and

naphthalene are given in the Supplementary Information.

Figure 2a shows an STM image of the Au(111) surface after deposition of 1 ML of pentacene molecules at RT. The pentacene molecules self-assemble into well-ordered islands, as previously reported.[34] Post-annealing this system at 525 K under UHV conditions induces the molecular desorption of the vast majority of molecules (Figure 2b), in good agreement with reported thermal programmed desorption (TPD) experiments.[35] Importantly, upon annealing, pentacene molecules do not undergo any coupling reaction; only some monomers remain on the surface, mainly located at the elbows of the herringbone reconstruction.[36] At this point, it should be noted that the inverted appearance of the reconstruction pattern in STM images in Figure 2b is characteristic of tip-induced motion of isolated molecules along the FCC regions of the herringbone reconstruction.[37]

This scenario changes completely when the annealing of the pentacene layer is carried out in the presence of atomic hydrogen (Figure 2d). A significant increase in the amount of pentacene molecules remaining on the Au(111) surface is observed, in marked contrast to the cases without hydrogen or with molecular hydrogen (Figures 2b and 2c, respectively). Importantly, the number of molecules remaining on the surface –and thus the reaction yield– depends on the amount of atomic hydrogen supplied to the system, suggesting that under such experimental conditions the extent of available H is the rate limiting factor (Figure 2e). A close-up view to the so-formed, homogeneously distributed molecular nanostructures reveals that they are composed of pentacene molecules arranged into dendritic covalently bonded structures (Figure 3). This assignment is supported by different experimental evidences. Firstly, the observed nanostructures remain intact after a 15 nm displacement and a 90º rotation induced by atomic manipulation with the STM tip (red circle in Figure S1). Secondly, these nanostructures exhibit a rather homogeneous appearance, in good agreement with superimposed (properly scaled) molecular models (Figure 3).

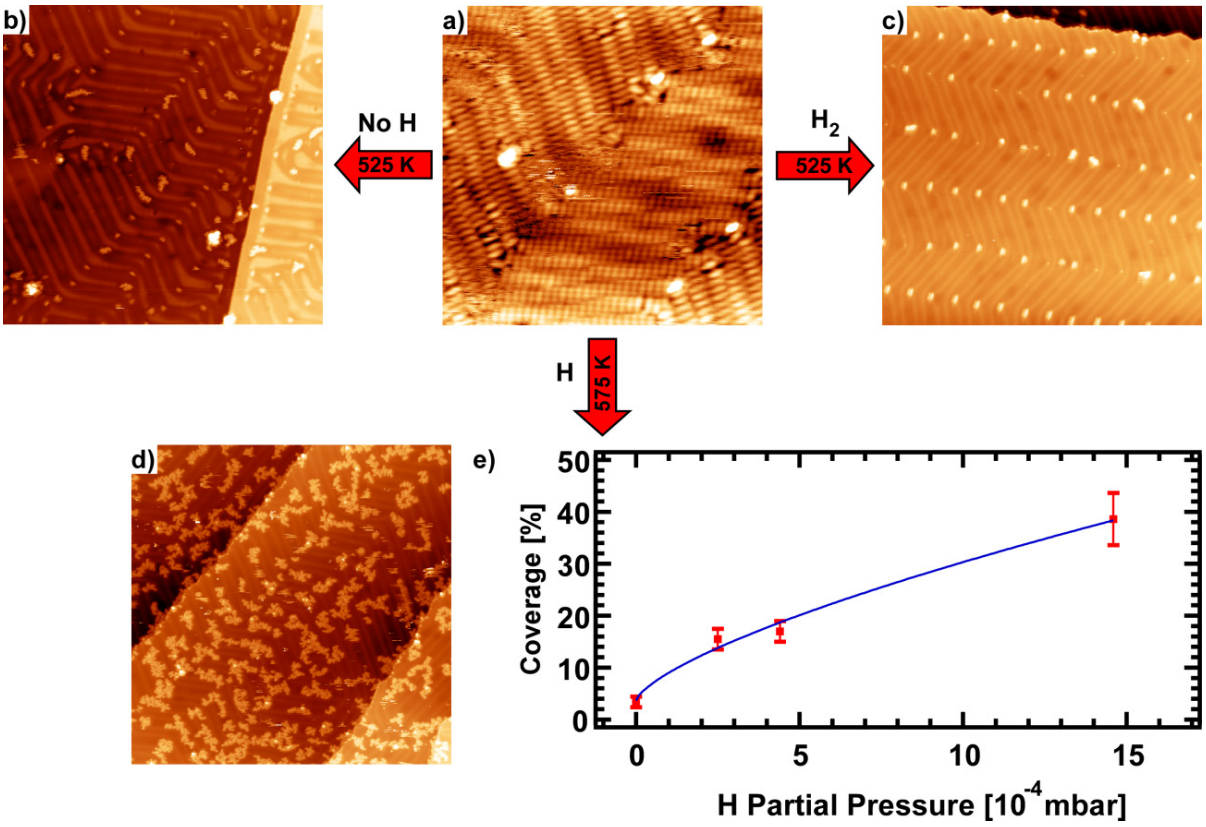

Figure 2.- Evolution of 1 ML pentacene on Au(111) with surface temperature and hydrogen partial pressure. **a)** STM image of the as-deposited molecular layer. Individual elongated features correspond to pentacene molecules which self-assemble into two domains following the herringbone reconstruction. STM parameters: 30 nm x 30 nm, I = 20 pA, V = -1.4 V, 77 K. **b)** STM image of the pentacene layer after annealing at 525 K in UHV. Most molecules have desorbed from the Au surface. STM parameters: 100 nm x 100 nm, I = 20 pA, V = -1.5 V, 77 K. **c)** STM image of the pentacene layer after annealing at 525 K in H_2 atmosphere ($P(H_2)$=1.5 10^{-3} mbar at the exit of the cracker capillary, H_2 cracker OFF). Again, most molecules have desorbed from the Au surface. STM parameters: 100 nm x 100 nm, I = 20 pA, V = -1.5 V. **d)** STM image of the pentacene layer after annealing at 525 K in the presence of atomic hydrogen (P(H)=1.5 10^{-3} mbar at the exit of the cracker capillary) and post-annealing at 575 K without further H supply. Pentacene-derived nanostructures appear on the surface as a consequence of intermolecular covalent coupling. STM parameters: 100 nm x 100 nm, I = 20 pA, V = -1.5 V. **e)** Graph showing the evolution of the surface coverage of pentacene-derived nanostructures with the estimated hydrogen partial pressure at the exit of the cracker capillary (cracker-sample separation ~ 10 cm). The blue line corresponds to a power-law fit to the experimental data (exponent=0.697). The value found at 0 partial pressure is due to reactions taking place at the elbows of the herringbone reconstruction. Error bars were estimated from the counting of not well-defined structures.

Figures 3a-f show a set of high-resolution STM images of some of the most characteristic and interesting molecular entities formed: L-shaped dimers (blue arrows), boomerang-shaped dimers (pink arrows), tetramers, and two rectangular structures (green and red arrows). The L-shaped dimer is proposed to be the result of the

covalent coupling of two pentacene molecules at C_1 positions (Figure 1a). Given the flexibility of the single C-C bond formed between the two pentacene molecules, the intermolecular angle can adopt different values depending on the surrounding structures and the registry with the surface. As an example, the L-shaped dimer in Figure 3a presents an angle of ~90º while the one in panel c is ~120º. In both cases, a good agreement between experimental STM image and the schematic scaled model is obtained (Figures 3b and 3d). On the other hand, the boomerang–shaped dimer may derive from the covalent coupling at C_1 and C_2 positions (Figures 3d and 3f). In this case, the angle between molecular axes is ~150º. The tetramer is compatible with the covalent coupling of an L-shaped and boomerang-shaped dimers as shown in Figure 3b. Finally, we have the rectangular structures which are probably the most interesting ones (Figures 3e and 3f). They are assigned to nano-graphene patches formed upon in-registry side-by-side intermolecular coalescence of two (red arrow) or three (green arrows) pentacene molecules (see Figure S4 for further details on their formation mechanism). Given their 0D character and their atomic structural precision, these nano-graphenes are expected to present intriguing electronic and magnetic properties such as giant edge state splitting localized at the zigzag edges.[38] Interestingly, the yield of nano-graphene formation is quite high, resulting in about 1 nano-graphene per 60 nm^2.

There are, of course, other examples for the on-surface synthesis of atomically precise nano-graphenes, such as e.g. the surface-assisted intramolecular cyclo-dehydrogenation of PAHs on metallic surfaces.[25–28] Additionally, the lateral coalescence of graphene-based nanostructures has also been reported, but it usually requires temperatures in excess of 650 K.[39,40] However, to the best of our knowledge, the structures reported here are the first examples of atomically precise nano-graphenes realized *via* on-surface coalescence of unsubstituted PAHs on rather inert substrates such as Au(111). Furthermore, our hydrogen-assisted strategy decreases the intermolecular coupling temperature by at least 125 K; that is, a 20 % with respect to other available protocols.

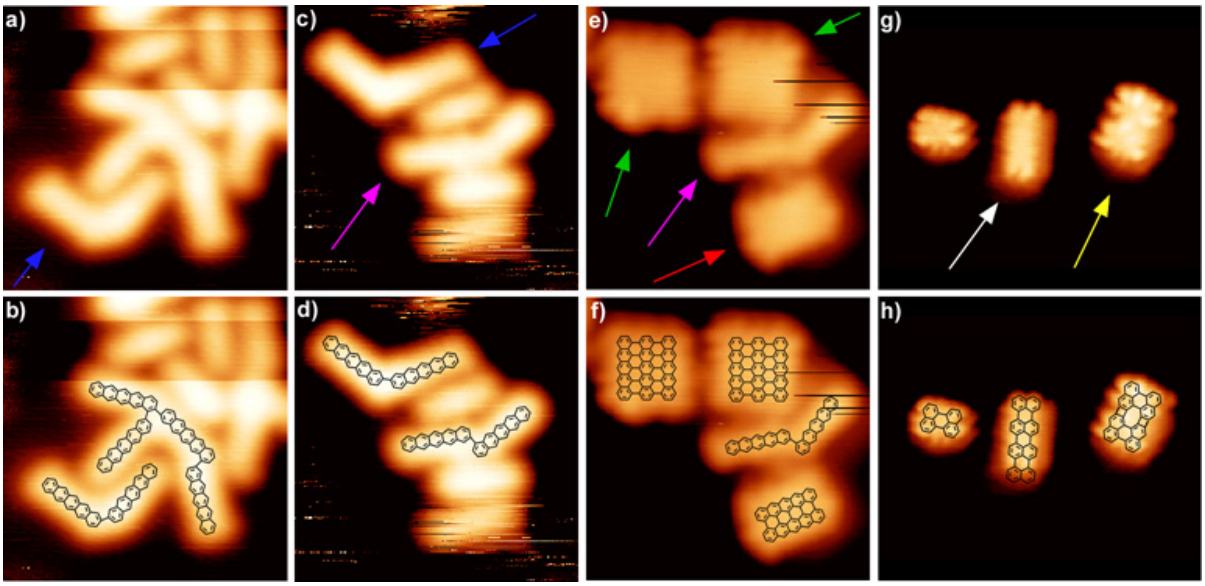

Figure 3.- STM images and schematic models for different pentacene- and perylene-derived nanostructures formed upon annealing in the presence of atomic hydrogen. **a,b)** L-shaped pentacene dimer (blue arrow) and pentacene tetramer formed upon C-C covalent coupling at C_1 (former), and C_1 and C_2 (latter) positions. STM parameters: 5.0 nm x 5.0 nm, I = 30 pA, V = -1.5 V, 77 K. **c,d)** L- and boomerang-shaped (blue and pink arrows, respectively) pentacene dimers formed after activation of C_1-C_1 and C_1-C_2 positions, respectively. STM parameters: 5.0 nm x 5.0 nm, I = 20 pA, V = -1.5 V, 77 K. **e,f)** Boomerang-shaped pentacene dimer (pink arrow) and rectangular patches (red and green arrows), the latter appearing upon in-registry lateral coalescence of two and three pentacene molecules, respectively. STM parameters: 5.0 nm x 5.0 nm, I = 20 pA, V = -1.5 V, 77 K. **g,h)** Perylene monomer (left) and dimers. The left dimer (white arrow) corresponds to the head-to-head covalent coupling of C'_1 carbon atoms while the right dimer (yellow arrow) is associated to the lateral fusion of two perylene molecules involving positions C'_2 and C'_3. STM parameters: 6.0 nm x 7.8 nm, I = 20 pA, V = -1.2 V, 5 K.

It is worthy to note that the methodology here presented can also be satisfactorily applied to the fabrication of pentacene-based nanostructures at even lower sample temperatures. Figures S2a,b show a set of STM images acquired upon annealing a pentacene/Au(111) sample at 425 K in the presence of atomic hydrogen. Despite the substantial decrease in sample temperature during the process, we can observe the formation of dendritic pentacene-derived nanostructures, as highlighted by blue arrows. This annealing temperature is around the desorption temperature of pentacene on Au(111) as mentioned above, and therefore there are still unreacted molecules diffusing on the surface, evidenced by the horizontal spikes in the STM images. In order to discern the real coverage of reacted molecules and to improve the quality of the images we desorbed unreacted pentacene, annealing at 525 K without further supply of atomic H. Figures S2c,d present the STM images obtained after such an annealing, where the formation of nanostructures similar to those presented in Figure 3 are observed, although with an obvious descent in the total amount of reacted molecules, which is approximately reduced by

50 %. This result further corroborates the existence of a rather low activation barrier which we propose to be associated to the essential super-hydrogenation step.

To check the versatility of this process, we have carried out experiments using perylene on Au(111). Perylene has been chosen because it combines armchair- and zigzag-edge topologies in similar proportion (Figure 1a). It has been suggested that zigzag edges in graphene-based nanostructures are more reactive than armchair ones due to the presence of electronic states close to the Fermi level.[41] This could induce selectivity in the H-mediated dehydrogenation of the molecule. We show in Figures 3g and S3 that our mechanism is also valid for perylene and leads to the formation of higher order molecules as a result of the H-induced intermolecular covalent coupling. Figure 3g shows an STM image of some interesting and characteristic nanostructures, namely a monomer and two dimers made of perylene units. High-resolution imaging of the monomer allows unambiguous determination of the molecular orientation; the two maxima at the edges corresponding to the zigzag edge. Thus, we can univocally assign the two dimers to an edge-to-edge fusion of two monomers, i.e., the formation of nano-graphenes; the one in the centre (white arrow) resulting from coalescence along the zigzag edge, while the one on the right (yellow arrow) coming along the armchair edge. This latter case is especially interesting as it implies the formation of an octagonal and two square rings, similar to the structures reported by M. Liu *et al*.[42] but without any need for molecular functionalization. Our results indicate that the process does no present selectivity towards any of the edges, indicating that the reactivity of the edge is not directly involved in the coupling mechanism.

As already introduced, the idea behind this work is to exploit the enhanced reactivity of activated intermediates to facilitate the formation of new covalent C-C bonds between PAHs. In our case, radical-like intermediate species are created by the super-hydrogenation of the PAHs upon exposure to atomic hydrogen on a surface. In order to corroborate our hypothesis and experimental observations, we have performed extensive Density Functional Theory (DFT) calculations to determine the energy barriers and enthalpies involved in the process. Attending to the proposed model and the experimental findings herein presented, we expect the following elements in the mechanism: (1) the reaction requires the presence of super-hydrogenated species created by exposure to atomic hydrogen; (2) it needs a surface to confine the species involved in the reaction –PAHs and atomic H– increasing the encounter probability in comparison to the gas phase, which explains why such a dehydrogenation process has not been observed in the gas phase;[7] and (3) it is expected to be thermally activated. Our calculations focus on the pentacene/Au(111) system, although we have also computed the most relevant steps for the naphthalene/Au(111) and perylene/Au(111) systems, which revealed no important differences (see Supplementary Information).

Following the experimental protocol, first a H atom approaches a pentacene molecule physisorbed on the Au surface (top left panel in Figure 4). When the H atom is close enough, two main possibilities arise: (1) it interacts with one of the pentacene peripheral H atoms, cleaves the C-H bond, and forms an H_2 molecule and a carbon radical, either in a Eley-Rideal or in a Langmuir-Hinshelwood mechanism;[43] or (2) it interacts with one of the C atoms and forms a chemical bond, super-hydrogenating the molecule and inducing a local sp^2-sp^3 transition (Figure 4, bottom left panel). The computed energy barriers for the different peripheral C atoms in cases (1) and (2) are in the range of 0.64-0.74 eV and 0.24-0.26 eV, respectively, the lower values corresponding to position C_4 (see Fig. 1a). This site-dependence energy barrier is in good agreement with the well-known higher reactivity of acenes at their more aromatic central rings.[44] Processes (1) and (2) compete, but molecular super-hydrogenation will prevail given the lower energy barrier, thus favoring the formation of the super-hydrogenated species, a key intermediate step prior to PAH intermolecular covalent coupling, as confirmed by control experiments (see Supplementary Information).

At this point, it is worthy to mention that molecular super-hydrogenation has to compete with the opposite process: the H-assisted cleavage of one of the C-H bonds of the super-hydrogenated molecular carbon atom, returning the molecule to its canonical form, e.g., $C_{22}H_{15} + H \rightarrow C_{22}H_{14} + H_2$. Such a process has a computed energy barrier in the range between 0.6 and 0.9 eV (see Figure S5), depending on the different C positions, and a net enthalpy gain in the range from 1.5 to 1.7 eV (exothermic). The efficiency of this process increases with the temperature, and is highly probable in the temperature range used in the experiments. However, its influence in the reaction mechanism will be limited as the experiments take place under a continuous flux of atomic H which will continuously replace the cleaved H.

Once the pentacene molecule is super-hydrogenated, i.e. in its radical-like state (bottom left panel in Figure 4), it shows an enhanced reactivity at contiguous C-H sites due to the local breaking of π-aromaticity. Consequently, two super-hydrogenated pentacene molecules find favorable to align (Figure 4, bottom middle panel) and join at their radical-like sites next to the super hydrogenated ones (Figure 4, top right panel), forming a new covalent C-C bond across the two molecules and the resulting super-hydrogenated pentacene dimer (Figure 4, bottom right panel).

Finally, in a last step, the dimer will *desuper-hydrogenate* –lose the extra H atoms– to return to its canonical form. This can occur assisted by an incoming H atom from the vacuum or the surface, in a pathway already sketched above. It should be noted that, as we are dealing with a large PAH, we may have different energetic scenarios depending on the super-hydrogenation site. For the sake of clarity, the energy curve in Figure 4 shows

the energy landscape for the most favorable situation in which pentacene molecules are super-hydrogenated at C_2 positions and couple at C_1 positions, i.e. C_1^2 –from now on we will name it as C_x^y, where *x* and *y* are the coupling and super-hydrogenation positions, respectively. In this case, the computed energy barrier for the C-C bond formation is 0.81 eV, a value that can be reasonably well overcome within the experimental conditions used in this work. Furthermore, the overall process is thermodynamically favored (exothermic), with an overall energy gain of 3.38 eV. Table S1 in Supporting Information shows the computed energy barriers and enthalpy gains for other favorable positions for pentacene and naphthalene. The small energy barrier differences among the super-hydrogenation and reaction sites for the inequivalent C atoms explain the lack of selectivity in the shape of the final nanostructures experimentally observed. Interestingly, the L type and boomerang-shaped dimers are the most frequently found and those with lower barriers and higher energy gains. Other *a priori* plausible situations not included in the table have been neglected as we deem them more unlikely attending to steric repulsion arguments. For example, $C_3^4 - C_3^4$, $C_4^3 - C_4^3$, or $C_3^4 - C_4^3$ can be excluded as hydrogen atoms in the edge of the molecule will repel each other, thus decreasing the efficiency of the process at central molecular positions. This effect has been observed for other acenes activated at central positions where no intermolecular covalent C-C bonds can be obtained and organometallic complexes, which present longer bonding distances, are achieved.[45] However, as shown in Figure 3e, it is possible to find nano-graphenes. We attribute their synthesis to a "zipping" process in which two or more pentacene molecules consecutively covalently bind from an initial C-C bond at C_2 positions (see Supplementary Information for further details on the "zipping" mechanism, Figure S4). Formation of other type of C-C bonds, as fused rings (five-membered ring for L-structures), although cannot be discarded, are unlike due to the molecular rigidity and that the process shall involve multiple super-hydrogenated sites.

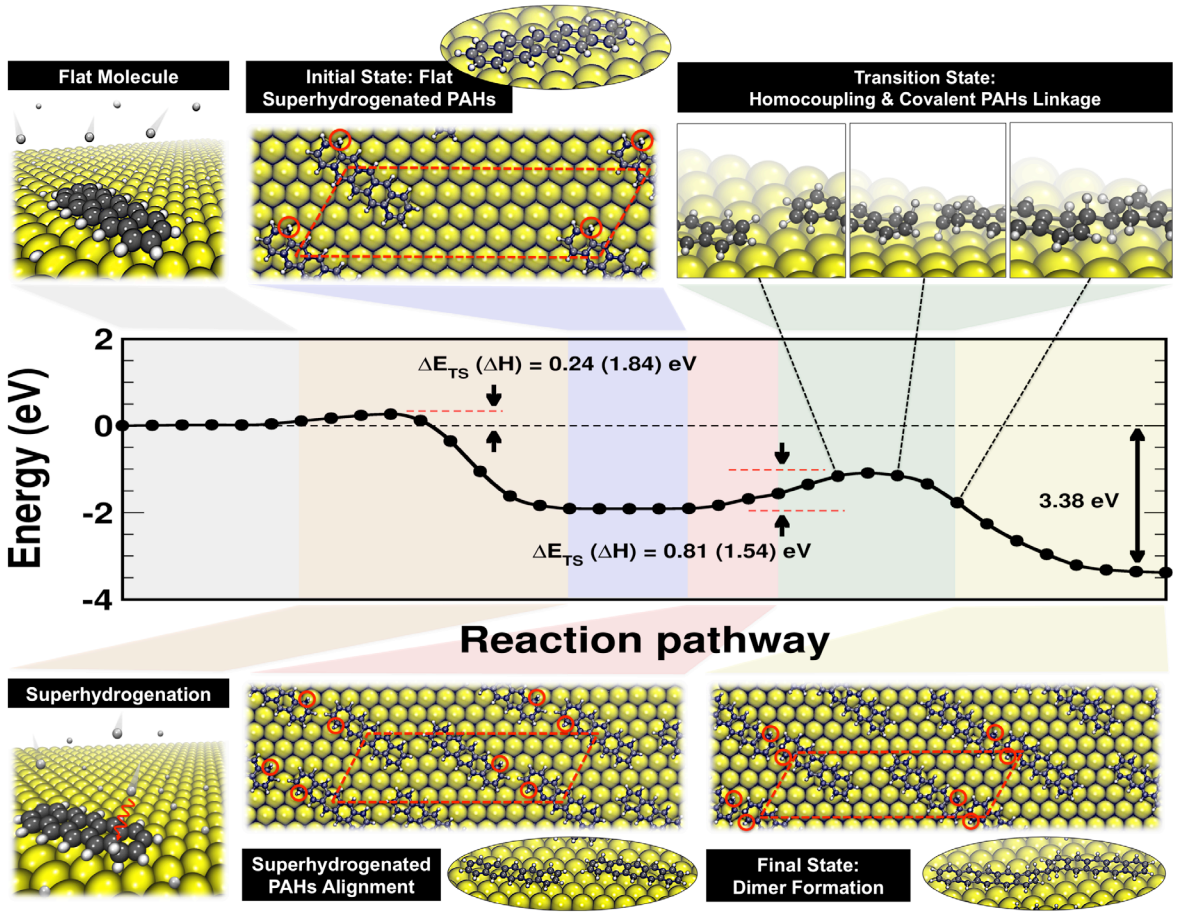

Figure 4.- Dimer formation involving C_1^2 positions *via* H-induced super-hydrogenation and intermolecular covalent C-C bond formation on Au(111) from CI-NEB calculations. **Top and bottom:** schematic representation of the most important steps involved in the reaction pathway. Yellow, dark grey, and white atoms correspond to Au, C, and H, respectively. Red dashed-line boxes superimposed in top views represent the simulation cells used in the calculations. Red circles highlight the C atoms where the super-hydrogenation takes place. **Middle:** energy diagram associated to the lowest barrier reaction pathway. Shading colors refer to the different steps of the reaction.

Although the mechanism here presented lacks, a priori, of selectivity, the comprehension of the atomistic mechanism and the appearance of highly reactive positions may lead to selectivity *via* the synthesis of tailored molecular precursors or by the introduction of heteroatoms at specific sites that may present a high affinity towards super-hydrogenation.[46]

Conclusions

Summarizing, we report on an atomistic mechanism leading to the activation and subsequent covalent coupling of organic molecules into higher order molecular nanostructures on surfaces. It is based on the adsorption of at

least an extra H atom at one of the molecular peripheral C atoms (super-hydrogenation), thus inducing a local sp^3–like configuration that locally breaks aromaticity, enhancing reactivity. Then, a new covalent C-C bond and two H_2 molecules are formed upon collision of two super-hydrogenated molecules at contiguous radical-like sites. The so-formed species continue aggregating, yielding characteristic dendritic nanostructures. Within the variety of so-formed nanostructures, a non-negligible amount of structurally well-defined nano-graphene is obtained upon side-by-side coalescence of two or more activated pentacene or perylene molecules.

Projecting these ideas, one could speculate how the proposed mechanism might be responsible for the formation of large aromatic species in circumstellar environments on the surface of dust grains that acts as a template rather than a catalyst.[6] Additionally, it opens a door to a new way of inducing dehydrogenation and covalent coupling of organic molecules on relatively inert surfaces, otherwise unattainable due to molecular desorption prior to reaction. Moreover, we speculate that a correct choice of the molecular precursors may enhance selectivity and make this strategy valuable for the non-Ullmann coupling of atomically controlled nanostructures, and with no undesired secondary products. We envision that, given the templating and hosting role of the surface, the proposed mechanism is quite general and could be reasonably applied to a wide range of PAHs adsorbed on diverse surfaces. Furthermore, we have found no arguments against the mechanism being extensible to more technologically-relevant substrates such as semiconductors or insulators.

Methods

Experiments have been carried out in a UHV chamber with a base pressure of 1.0 10^{-10} mbar, equipped with an LT-STM (Scienta Omicron) and a thermal gas cracker (MGC Series, Mantis Deposition). Au(111) single crystal substrates (Surface Preparation Laboratory, Netherlands) were cleaned using the standard protocol based on repeated cycles of sputtering (Ar^+ ions, 1.0 kV) and annealing (~750 K) until judged clean by STM. Pentacene (Sigma Aldrich, 99+%) and perylene (Acros Organics, 98%) molecules were sublimed from a Kentax three-fold evaporator (Kentax GmbH) at a rate of ~1 $Åmin^{-1}$ (sublimation temperatures of 460 K and 400 K, respectively). Prior to deposition, they were thoroughly outgassed for several hours at temperatures 20 K lower than those used for deposition. STM images were acquired in the constant current mode. For the sample preparation, the following procedure was used: a full molecular monolayer was deposited on the clean Au(111) surface held at RT. Then the sample was faced toward the H_2 cracker and exposed to a flux of atomic H while ramping the sample temperature from RT to 525K in 10 minutes, and then kept at 525K for another 20 minutes. After that, the annealing was stopped and the sample was allowed to cool down to RT while keeping the atomic H flux

during the first 5 minutes. The partial pressure of H_2 in the chamber during H exposure was 5.0 10^{-7} mbar unless otherwise stated, and the working power of the hydrogen cracker was 40 W. Using these parameters, we estimate a cracking efficiency of around 40-50% and a pressure in the capillary around 4 orders of magnitude higher than that in the chamber. All temperatures were measured with an infrared pyrometer (Optris) using an emissivity of ε=0.1.

Atomic mechanisms for our experiments are based on *ab-initio* Density Functional Theory.[47] Both extended[48] and localised[49] models have been used, the former mainly appropriate for periodic systems like the gold surface, the latter primarily adapted to small clusters of atoms like molecules. Comparison of values calculated with such different basis for similar models, whenever it has been possible, yields confidence on the generality and consistency of our results. Total internal electronic energies for self-consistent states of stationary configurations (both local minima and kinetic barriers) have been computed. Different convergence thresholds and parameters controlling the accuracy of the calculations are given in the supplementary information.

Corresponding Authors

cssanchez@icmm.csic.es

gago@icmm.csic.es

Acknowledgements

This work was supported by the Spanish MINECO (Grant MAT2017-85089-C2-1-R), the Swiss National Science Foundation, and the EU via the ERC-Synergy Program (Grant No. ERC-2013-SYG-610256 NANOCOSMOS) and the Innovation Program (Grant 696656: Graphene Core1. Graphene-based disruptive technologies). JIM acknowledges support from Ramón y Cajal Program (Grant RYC-2015-17730), as well as computing resources from CTI-CSIC. CS-S is grateful to Ministerio de Economía y Competitividad for financial support via the Juan de la Cierva Incorporación grant (IJCI-2014-19291, co-funded by the European Investment Bank). We thank Dra. Araceli González Campaña and Prof. Diego Peña for fruitful discussion.

Supporting Information Available: Manipulation experiments, the perylene case, calculations of energy barriers and enthalpies for other configurations, the "Zipping" mechanism for the formation of nanographene patches upon side-by-side coalescence of pentacene molecules, super-hydrogenation of PAHs, activation and covalent coupling of pentacene super-hydrogenated at RT, and Density Functional Theory Modelling. This material is available free of charge *via* the Internet at http://pubs.acs.org.

References

(1) Blumer, M. Polycyclic Aromatic Compounds in Nature. *Sci. Am.* **1976**, *234*, 34–45.

(2) Gentry, J. C. Benzene Production and Economics: A Review. *Asia-Pac. J. Chem. Eng.* **2007**, *2* (4), 272–277.

(3) Haritash, A. K.; Kaushik, C. P. Biodegradation Aspects of Polycyclic Aromatic Hydrocarbons (PAHs): A Review. *J. Hazard. Mater.* **2009**, *169* (1–3), 1–15.

(4) Cook, D. J.; Schlemmer, S.; Balucani, N.; Wagner, D. R.; Steiner, B.; Saykally, R. J. Infrared Emission Spectra of Candidate Interstellar Aromatic Molecules. *Nature* **1996**, *380* (6571), 227–229.

(5) Tielens, A. G. G. M. Interstellar Polycyclic Aromatic Hydrocarbon Molecules. *Annu. Rev. Astron. Astrophys.* **2008**, *46* (1), 289–337.

(6) Merino, P.; Švec, M.; Martinez, J. I.; Jelinek, P.; Lacovig, P.; Dalmiglio, M.; Lizzit, S.; Soukiassian, P.; Cernicharo, J.; Martin-Gago, J. A. Graphene Etching on SiC Grains as a Path to Interstellar Polycyclic Aromatic Hydrocarbons Formation. *Nat. Commun.* **2014**, *5*.

(7) Montillaud, J.; Joblin, C.; Toublanc, D. Evolution of Polycyclic Aromatic Hydrocarbons in Photodissociation Regions: Hydrogenation and Charge States. *Astron. Astrophys.* **2013**, *552*, A15.

(8) Ehrenfreund, P.; Rasmussen, S.; Cleaves, J.; Chen, L. Experimentally Tracing the Key Steps in the Origin of Life: The Aromatic World. *Astrobiology* **2006**, *6* (3), 490–520.

(9) Wakelam, V.; Bron, E.; Cazaux, S.; Dulieu, F.; Gry, C.; Guillard, P.; Habart, E.; Hornekær, L.; Morisset, S.; Nyman, G.; Pirronello, V.; Price, S.D.; Valdivia, V.; Vidali, G.; Watanabe, N. H2 Formation on Interstellar Dust Grains: The Viewpoints of Theory, Experiments, Models and Observations. *Mol. Astrophys.* **2017**, *9*, 1–36.

(10) Thrower, J. D.; Jørgensen, B.; Friis, E. E.; Baouche, S.; Mennella, V.; Luntz, A. C.; Andersen, M.; Hammer, B.; Hornekær, L. Experimental Evidence for the Formation of Highly Superhydrogenated Polycyclic Aromatic Hydrocarbons Through H Atom Addition and Their Catalytic Role in H2 Formation. *Astrophys. J.* **2012**, *752* (1), 3.

(11) Vispute, T. P.; Zhang, H.; Sanna, A.; Xiao, R.; Huber, G. W. Renewable Chemical Commodity Feedstocks from Integrated Catalytic Processing of Pyrolysis Oils. *Science* **2010**, *330* (6008), 1222–1227.

(12) *Lange's Handbook of Chemistry*, 15. ed.; Dean, J. A., Lange, N. A., Eds.; McGraw-Hill handbooks; McGraw-Hill: New York, NY, 1999.

(13) *Encyclopedia of Catalysis*; Horváth, I. T., Ed.; John Wiley & Sons, INC., 2002.

(14) Galabov, B.; Nalbantova, D.; Schleyer, P. von R.; Schaefer, H. F. Electrophilic Aromatic Substitution: New Insights into an Old Class of Reactions. *Acc. Chem. Res.* **2016**, *49* (6), 1191–1199.

(15) de Oteyza, D. G.; Gorman, P.; Chen, Y.-C.; Wickenburg, S.; Riss, A.; Mowbray, D. J.; Etkin, G.; Pedramrazi, Z.; Tsai, H.-Z.; Rubio, A.; Crommie, M.F.; Fischer, F.R.. Direct Imaging of Covalent Bond Structure in Single-Molecule Chemical Reactions. *Science* **2013**, *340* (6139), 1434–1437.

(16) Gourdon, A. On-Surface Covalent Coupling in Ultrahigh Vacuum. *Angew. Chem. Int. Ed.* **2008**, *47* (37), 6950–6953.

(17) Fan, Q.; Gottfried, J. M.; Zhu, J. Surface-Catalyzed C–C Covalent Coupling Strategies toward the Synthesis of Low-Dimensional Carbon-Based Nanostructures. *Acc. Chem. Res.* **2015**, *48* (8), 2484–2494.

(18) Dong, L.; Liu, P. N.; Lin, N. Surface-Activated Coupling Reactions Confined on a Surface. *Acc. Chem. Res.* **2015**, *48* (10), 2765–2774.

(19) Shen, Q.; Gao, H.-Y.; Fuchs, H. Frontiers of On-Surface Synthesis: From Principles to Applications. *Nano Today* **2017**, *13*, 77–96.

(20) Otero, G.; Biddau, G.; Sánchez-Sánchez, C.; Caillard, R.; López, M. F.; Rogero, C.; Palomares, F. J.; Cabello, N.; Basanta, M. A.; Ortega, J.; Méndez, J.; Echavarren, A.M.; Pérez, R.; Gómez-Lor, B.; Martín-Gago, J.A. Fullerenes from Aromatic Precursors by Surface-Catalysed Cyclodehydrogenation. *Nature* **2008**, *454* (7206), 865–868.

(21) Amsharov, K.; Abdurakhmanova, N.; Stepanow, S.; Rauschenbach, S.; Jansen, M.; Kern, K. Towards the Isomer-Specific Synthesis of Higher Fullerenes and Buckybowls by the Surface-Catalyzed Cyclodehydrogenation of Aromatic Precursors. *Angew. Chem. Int. Ed.* **2010**, *49* (49), 9392–9396.

(22) Sanchez-Valencia, J. R.; Dienel, T.; Gröning, O.; Shorubalko, I.; Mueller, A.; Jansen, M.; Amsharov, K.; Ruffieux, P.; Fasel, R. Controlled Synthesis of Single-Chirality Carbon Nanotubes. *Nature* **2014**, *512* (7512), 61–64.

(23) Rim, K. T.; Siaj, M.; Xiao, S.; Myers, M.; Carpentier, V. D.; Liu, L.; Su, C.; Steigerwald, M. L.; Hybertsen, M. S.; McBreen, P. H.; Flynn, G.W.; Nuckolls, C. Forming Aromatic Hemispheres on Transition-Metal Surfaces. *Angew. Chem. Int. Ed.* **2007**, *46* (41), 7891–7895.

(24) Sánchez-Sánchez, C.; Martínez, J. I.; Lanzilotto, V.; Biddau, G.; Gómez-Lor, B.; Pérez, R.; Floreano, L.; López, M. F.; Martín-Gago, J. Á. Chemistry and Temperature-Assisted Dehydrogenation of C60H30 Molecules on TiO2(110) Surfaces. *Nanoscale* **2013**, *5* (22), 11058–11065.

(25) Simonov, K. A.; Vinogradov, N. A.; Vinogradov, A. S.; Generalov, A. V.; Zagrebina, E. M.; Svirskiy, G. I.; Cafolla, A. A.; Carpy, T.; Cunniffe, J. P.; Taketsugu, T.; Lyaling, A.; Martensson, N.; Preobajenski, A.B. From Graphene Nanoribbons on Cu(111) to Nanographene on Cu(110): Critical Role of Substrate Structure in the Bottom-Up Fabrication Strategy. *ACS Nano* **2015**, *9* (9), 8997–9011.

(26) Sánchez-Sánchez, C.; Dienel, T.; Deniz, O.; Ruffieux, P.; Berger, R.; Feng, X.; Müllen, K.; Fasel, R. Purely Armchair or Partially Chiral: Noncontact Atomic Force Microscopy Characterization of Dibromo-Bianthryl-Based Graphene Nanoribbons Grown on Cu(111). *ACS Nano* **2016**, *10* (8), 8006–8011.

(27) Treier, M.; Pignedoli, C. A.; Laino, T.; Rieger, R.; Müllen, K.; Passerone, D.; Fasel, R. Surface-Assisted Cyclodehydrogenation Provides a Synthetic Route towards Easily Processable and Chemically Tailored Nanographenes. *Nat. Chem.* **2011**, *3* (1), 61–67.

(28) Pinardi, A. L.; Otero-Irurueta, G.; Palacio, I.; Martinez, J. I.; Sanchez-Sanchez, C.; Tello, M.; Rogero, C.; Cossaro, A.; Preobrajenski, A.; Gómez-Lor, B.; Jancarik, A.; Stará, I.G.; Starý, I; López, M.F.; Méndez, J.; Martín-Gago, J.A. Tailored Formation of N-Doped Nanoarchitectures by Diffusion-Controlled on-Surface (Cyclo)Dehydrogenation of Heteroaromatics. *ACS Nano* **2013**, *7* (4), 3676–3684.

(29) Pavliček, N.; Mistry, A.; Majzik, Z.; Moll, N.; Meyer, G.; Fox, D. J.; Gross, L. Synthesis and Characterization of Triangulene. *Nat. Nanotechnol.* **2017**, *12* (4), 308–311.

(30) Ruiz del Árbol, N.; Palacio, I.; Otero-Irurueta, G.; Martínez, J. I.; de Andrés, P. L.; Stetsovych, O.; Moro-Lagares, M.; Mutombo, P.; Svec, M.; Jelínek, P.; Cossaro, A.; Floreano, L.; Ellis, G.J.; López, M.F.; Martín-Gago, J.A. On-Surface Bottom-Up Synthesis of Azine Derivatives Displaying Strong Acceptor Behavior. *Angew. Chem. Int. Ed.* **2018**, *57* (28), 8582–8586.

(31) Talirz, L.; Ruffieux, P.; Fasel, R. On-Surface Synthesis of Atomically Precise Graphene Nanoribbons. *Adv. Mater.* **2016**, *28* (29), 6222–6231.

(32) Sánchez-Sánchez, C.; Brüller, S.; Sachdev, H.; Müllen, K.; Krieg, M.; Bettinger, H. F.; Nicolaï, A.; Meunier, V.; Talirz, L.; Fasel, R.; Ruffieux, P. On-Surface Synthesis of BN-Substituted Heteroaromatic Networks. *ACS Nano* **2015**, *9* (9), 9228–9235.

(33) Batzill, M. The Surface Science of Graphene: Metal Interfaces, CVD Synthesis, Nanoribbons, Chemical Modifications, and Defects. *Surf. Sci. Rep.* **2012**, *67* (3–4), 83–115.

(34) France, C. B.; Schroeder, P. G.; Parkinson, B. A. Direct Observation of a Widely Spaced Periodic Row Structure at the Pentacene/Au(111) Interface Using Scanning Tunneling Microscopy. *Nano Lett.* **2002**, *2* (7), 693–696.

(35) France, C. B.; Schroeder, P. G.; Forsythe, J. C.; Parkinson, B. A. Scanning Tunneling Microscopy Study of the Coverage-Dependent Structures of Pentacene on Au(111). *Langmuir* **2003**, *19* (4), 1274–1281.

(36) Chambliss, D. D.; Wilson, R. J.; Chiang, S. Nucleation of Ordered Ni Island Arrays on A(111) by Surface-Lattice Dislocations. *Phys. Rev. Lett.* **1991**, *66* (13), 1721.

(37) Böhringer, M.; Morgenstern, K.; Schneider, W.-D.; Berndt, R. Reversed Surface Corrugation in STM Images on Au(111) by Field-Induced Lateral Motion of Adsorbed Molecules. *Surf. Sci.* **2000**, *457* (1–2), 37–50.

(38) Wang, S.; Talirz, L.; Pignedoli, C. A.; Feng, X.; Müllen, K.; Fasel, R.; Ruffieux, P. Giant Edge State Splitting at Atomically Precise Graphene Zigzag Edges. *Nat. Commun.* **2016**, *7*, 11507.

(39) Basagni, A.; Sedona, F.; Pignedoli, C. A.; Cattelan, M.; Nicolas, L.; Casarin, M.; Sambi, M. Molecules–Oligomers–Nanowires–Graphene Nanoribbons: A Bottom-Up Stepwise On-Surface Covalent Synthesis Preserving Long-Range Order. *J. Am. Chem. Soc.* **2015**, *137* (5), 1802–1808.

(40) Deniz, O.; Sánchez-Sánchez, C.; Dumslaff, T.; Feng, X.; Narita, A.; Müllen, K.; Kharche, N.; Meunier, V.; Fasel, R.; Ruffieux, P. Revealing the Electronic Structure of Silicon Intercalated Armchair Graphene Nanoribbons by Scanning Tunneling Spectroscopy. *Nano Lett.* **2017**, *17* (4), 2197–2203.

(41) Jiang, D.; Sumpter, B. G.; Dai, S. Unique Chemical Reactivity of a Graphene Nanoribbon's Zigzag Edge. *J. Chem. Phys.* **2007**, *126* (13), 134701.

(42) Liu, M.; Liu, M.; She, L.; Zha, Z.; Pan, J.; Li, S.; Li, T.; He, Y.; Cai, Z.; Wang, J.; Zheng, Y.; Qiu, X.; Zhong, D. Graphene-like Nanoribbons Periodically Embedded with Four- and Eight-Membered Rings. *Nat. Commun.* **2017**, *8*, 14924.

(43) Somorjai, G. A. *Introduction to Surface Chemistry and Catalysis*; John Wiley & Sons, INC.: New York, NY, 1994.

(44) Schleyer, P. von R.; Manoharan, M.; Jiao, H.; Stahl, F. The Acenes: Is There a Relationship between Aromatic Stabilization and Reactivity? *Org. Lett.* **2001**, *3* (23), 3643–3646.

(45) Urgel, J. I.; Hayashi, H.; Di Giovannantonio, M.; Pignedoli, C. A.; Mishra, S.; Deniz, O.; Yamashita, M.; Dienel, T.; Ruffieux, P.; Yamada, H.; Fasel, R. On-Surface Synthesis of Heptacene Organometallic Complexes. *J. Am. Chem. Soc.* **2017**, *139* (34), 11658–11661.

(46) Hayashi, H.; Yamaguchi, J.; Jippo, H.; Hayashi, R.; Aratani, N.; Ohfuchi, M.; Sato, S.; Yamada, H. Experimental and Theoretical Investigations of Surface-Assisted Graphene Nanoribbon Synthesis Featuring Carbon–Fluorine Bond Cleavage. *ACS Nano* **2017**, *11* (6), 6204–6210.

(47) Hohenberg, P.; Kohn, W. Inhomogeneous Electron Gas. *Phys. Rev.* **1964**, *136* (3B), B864–B871.

(48) Giannozzi, P.; Baroni, S.; Bonini, N.; Calandra, M.; Car, R.; Cavazzoni, C.; Ceresoli, D.; Chiarotti, G. L.; Cococcioni, M.; Dabo, I.; Dal Corso, A.; de Gironcoli, S.; Fabris, S.; Fratesi, G.; Gabauer, R.; Gerstmann, U.; Gougoussis, C.; Kokalj, A.; Lazzeri, M.; Martin-Samos, L.; Marzari, N.; Mauri, F.; Mazzarello, R.; Paolini, S.; Pasquarello, A.; Paulatto, L.; Sbraccia, C.; Scandolo, S.; Sclauzero, G.; Seitsonen, A.P.; Smogunov, A.; Umari, P.; Wentzcovitch, R.M. QUANTUM ESPRESSO: A Modular and Open-Source Software Project for Quantum Simulations of Materials. *J. Phys. Condens. Matter* **2009**, *21* (39), 395502.

(49) Frisch, M. J.; Trucks, G. W.; Schlegel, H. B.; Scuseria, G. E.; Robb, M. A.; Cheeseman, J. R.; Scalmani, G.; Barone, V.; Petersson, G. A.; Nakatsuji, H.; Li, X.; Caricato, M.; Marenich, A.; Bloino, J.; Janesko, B.G.; Gomperts, R.; Mennucci, B.; Hratchian, H.P.; Ortiz, J.V.; Izmaylov, A.F.; Sonnenberg, J.L.; Williams-Young, D.; Ding, F.; Lipparini, F.; Egidi, F.; Goings, J.; Peng, B.; Petrone, A.; Henderson, T.; Ranasinghe, D.; Zakrzewski, V.G.; Gao, J.; Rega, N.; Zheng, G.; Liang, W.; Hada, M.; Ehara, M.; Toyota, K.; Fukuda, R.; Hasegawa, J.; Ishida, M.; Nakajima, T.; Honda, Y.; Kitao, O.; Nakai, H.; Vreven, T.; Throssell, K.; Montgomery, Jr., J.A.; Peralta, J.E.; Ogliaro, F.; Bearpark, M.; Heyd, J.J.; Brothers, E.; Kudin, K.N.; Staroverov, V.N.; Keith, T.; Kobayashi, R.; Normand, J.; Raghavachari, K.; Rendell, A.; Burant, J.C.; Iyengar, S.S.; Tomasi, J.; Cossi, M.; Millam, J.M.; Klene, M.; Adamo, C.; Cammi, R.; Ochterski, J.W.; Martin, R.L.; Morokuma, K.; Farkas, O.; Foresman, J.B.; Fox, D.J. *Gaussian 09 Rev. E.01*; Gaussian, INC: Wallingford, CT, 2009.

Table of Contents